Acta Crystallographica Section F
Structural Biology and Crystallization Communications
ISSN 1744-3091

Structures of native and Fe-substituted SOD2 from *Saccharomyces cerevisiae*

Yan Kang, Yong-Xing He, Meng-Xi Zhao and Wei-Fang Li*

School of Life Sciences, University of Science and Technology of China, Hefei, Anhui 230027, People's Republic of China

Correspondence e-mail: liwf@ustc.edu.cn

Received 5 May 2011
Accepted 19 July 2011

PDB References: SOD2, 3bfr; iron-substituted SOD2, 3rn4.

The manganese-specific superoxide dismutase SOD2 from the yeast *Saccharomyces cerevisiae* is a protein that resides in the mitochondrion and protects it against attack by superoxide radicals. However, a high iron concentration in the mitochondria results in iron misincorporation at the active site, with subsequent inactivation of SOD2. Here, the crystal structures of SOD2 bound with the native metal manganese and with the 'wrong' metal iron are presented at 2.05 and 1.79 Å resolution, respectively. Structural comparison of the two structures shows no significant conformational alteration in the overall structure or in the active site upon binding the non-native metal iron. Moreover, residues Asp163 and Lys80 are proposed to potentially be responsible for the metal specificity of the Mn-specific SOD. Additionally, the surface-potential distribution of SOD2 revealed a conserved positively charged electrostatic zone in the proximity of the active site that probably functions in the same way as in Cu/Zn-SODs by facilitating the diffusion of the superoxide anion to the metal ion.

1. Introduction

Oxygen plays a dual role in living organisms: although it helps in burning food to provide energy, it also undermines organisms by oxidizing their cell components. Superoxide radicals are one of the most notorious harmful byproducts of oxygen, but they can be quickly and efficiently eliminated in cells by superoxide dismutase (SOD; EC 1.15.1.1), an enzyme which can convert superoxide radicals into the less toxic H_2O_2 and O_2. Owing to its biological significance, SOD has been widely studied in various species at both the physiological and biochemical levels.

SOD2 is a manganese-specific SOD that resides in the mitochondrion (Luk *et al.*, 2003) and belongs to the highly conserved Mn/Fe-SOD family that adopt the α/β-fold and have either manganese or iron incorporated at the active site. The manganese or iron is invariably coordinated with distorted trigonal bipyramidal geometry by three histidines, one aspartate and a solvent molecule. The catalytic process consists of two half-reactions as seen in equations (1) and (2) (where M denotes the metal ion), in which the metal ion alternately oxidizes and reduces the $O_2^{-\cdot}$ anion. Therefore, the active-site reduction mid-point potential (E_m) must be finely tuned by the enzyme to efficiently drive the two half-reactions. An outer sphere hydrogen-bond network is also needed for the formation of hydrogen peroxide as shown in (2).

$$M^{3+}\text{-SOD}(OH^-) + O_2^{-\cdot} + H^+ \rightarrow M^{2+}\text{-SOD}(OH_2) + O_2 \quad (1)$$

$$M^{2+}\text{-SOD}(OH_2) + O_2^{-\cdot} + H^+ \rightarrow M^{3+}\text{-SOD}(OH)^- + H_2O_2. \quad (2)$$

Many members of the Mn/Fe-SOD family are only active with their respective metal ion at the active site, although they share high homology, do not show an obvious prominent preference for the cognate metal ion in the synthesis process and can have the active site misincorporated if synthesized in an environment with a higher concentration of the 'wrong' ion than the cognate ion (Beyer & Fridovich, 1991). Some members that do not show metal specificity

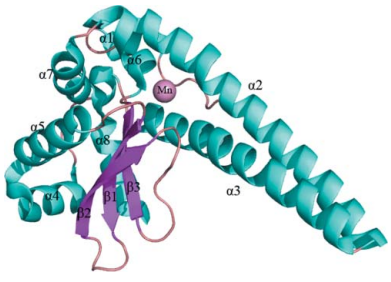

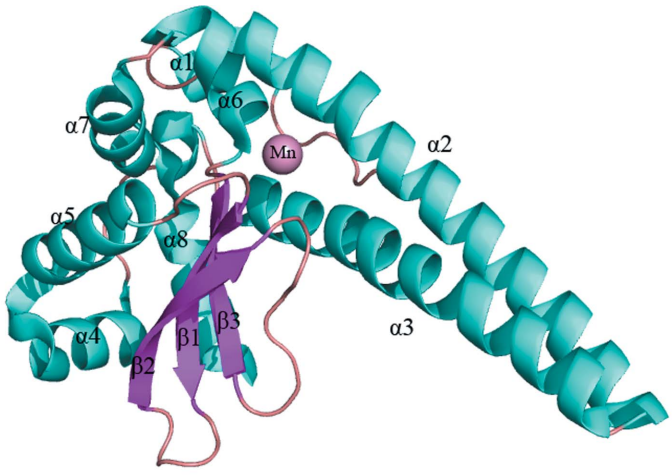

(*a*)

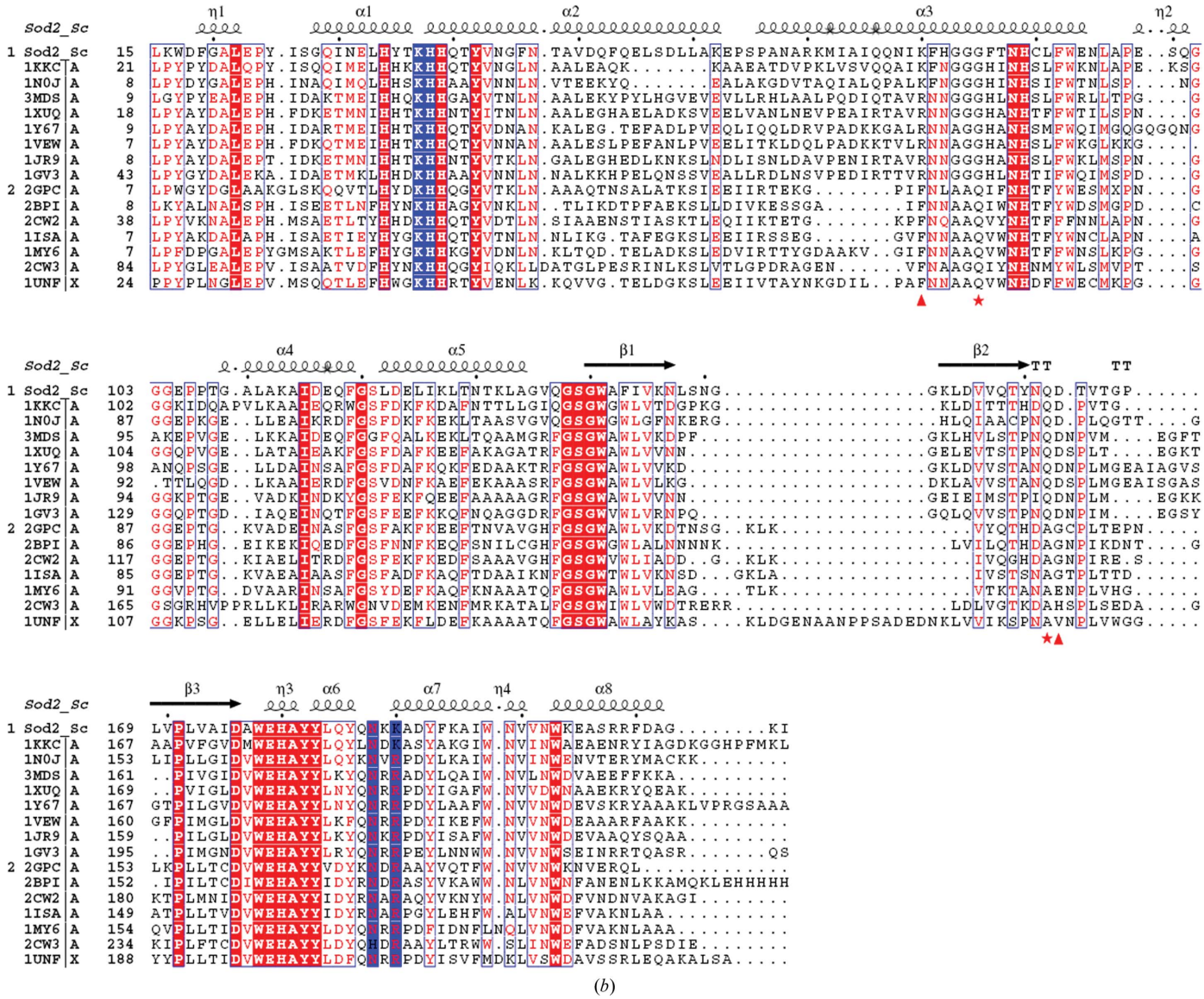

(*b*)

Figure 1
Structure of native SOD2 from *S. cerevisiae*. (*a*) Cartoon representation of SOD2; secondary-structural elements are annotated. (*b*) Multiple sequence alignment of SOD2 and members of the Mn/Fe-SOD family available in the PDB. Mn-specific SODs and Fe-specific SODs are grouped into groups 1 and 2, respectively. The residues governing the solvent W1 are marked with red stars and the hydrogen-bonding pairs specific to Mn-specific SODs are marked with red triangles. The residues that are responsible for the positively charged attractive zone are boxed in blue.

Table 1
Crystal parameters, data collection and structure refinement.

	Native SOD2	Fe-substituted SOD2
Data collection		
Space group	*P*23	*P*23
Unit-cell parameters (Å, °)	$a = b = c = 92.74$, $\alpha = \beta = \gamma = 90$	$a = b = c = 92.69$, $\alpha = \beta = \gamma = 90$
Resolution range (Å)	18.55–2.05 (2.10–2.05)	27.95–1.79 (1.89–1.79)
Unique reflections	16997	25311
Completeness (%)	99.9 (100.0)	99.9 (100.0)
$\langle I/\sigma(I)\rangle$	18.3 (5.2)	26.3 (11.5)
$R_{\rm merge}$† (%)	8.0 (37.6)	7.7 (20.5)
Average multiplicity	6.9	15.3
Refinement statistics		
Resolution range (Å)	15.00–2.05	27.95–1.79
R factor/$R_{\rm free}$‡ (%)	19.7/23.4	19.6/23.8
R.m.s.d. bond lengths/bond angles (°)	0.007/0.992	0.011/1.227
Average B factor (Å^2)	19.6	18.4
Ramachandran plot, residues in		
Most favourable regions (%)	96.46	98.00
Additional allowed regions (%)	3.54	2.00
PDB entry	3bfr	3rn4

† $R_{\rm merge} = \sum_{hkl}\sum_i |I_i(hkl) - \langle I(hkl)\rangle| / \sum_{hkl}\sum_i I_i(hkl)$, where $I_i(hkl)$ is the intensity of an observation and $\langle I(hkl)\rangle$ is the mean value for the unique reflection; summations are over all reflections. ‡ R factor $= \sum_{hkl} \big||F_{\rm obs}| - |F_{\rm calc}|\big| / \sum_{hkl} |F_{\rm obs}|$, where $F_{\rm obs}$ and $F_{\rm calc}$ are the observed and calculated structure-factor amplitudes, respectively. The free R factor was calculated with 5% of the data that were excluded from the refinement.

are named cambialistic SODs. In *Saccharomyces cerevisiae* the bulk of the mitochondrial iron is normally unavailable to SOD2; however, when mitochondrial iron homeostasis is disrupted by iron overload SOD2 is greatly inactivated. The ability to control homeostasis of the reactive iron pool in mitochondria is thought to have important implications for oxidative stress in disorders of iron overload (Yang *et al.*, 2006).

Here, we report crystal structures of SOD2 from *S. cerevisiae* bound with the native manganese and with the 'wrong' ion iron, respectively. Structural comparison revealed that Fe-substituted SOD2 has a very similar structure to that of native SOD2. The surface-potential distribution of SOD2 revealed a conserved positively charged electrostatic zone in the proximity of the active site that probably functions the same way as in the Cu/Zn-SODs.

2. Materials and methods

2.1. Cloning, purification and atomic absorption spectra

The DNA sequence of the mature form of SOD2 was amplified by PCR from genomic DNA of *S. cerevisiae* S288C and cloned into a pET28a-derived expression vector between *Nde*I and *Not*I restriction sites. There was an additional sequence coding for a hexahistidine just after the start codon. The plasmid containing *SOD2* was transformed into *Escherichia coli* BL21 (DE3) cells for expression. For native SOD2 expression, the transformant cells were grown in 2×YT medium (Oxoid Ltd) supplemented with 0.1 m*M* $MnCl_2$. For the Fe-substituted SOD2, the transformant cells were grown in M9 medium supplemented with 0.1 m*M* $FeCl_3$. When the cell culture reached an $OD_{600\,nm}$ of 0.6, protein expression was induced with 0.2 m*M* IPTG (BBI) and the cells were grown at 310 K for a further 4 h. The cells were collected by centrifugation, suspended in 30 ml buffer consisting of 20 m*M* Tris–HCl pH 8.0, 200 m*M* NaCl and stored overnight at 253 K. The cells were lysed by three cycles of freezing/thawing and sonication. The His-tagged proteins were purified on an Ni^{2+}–NTA (Amersham Biosciences) affinity column using standard protocols. The eluted protein was further purified by gel filtration on a Superdex 200 column (Amersham Biosciences) equilibrated with 20 m*M* Tris–HCl pH 7.5, 200 m*M* NaCl. The purity of the pooled fractions was checked by SDS–PAGE. The Fe content of the purified protein was determined by graphite furnace atomic absorption spectrometry (GFAAS) using an AAnalyst 800 Spectrometer (Perkin Elmer). The Mn content was determined by inductively coupled plasma atomic emission spectroscopy (ICP-AES) on an Atomscan Advantage (Thermo Jarrell Ash Corporation). The wavelengths for determination of Fe and Mn were set to 257.9 and 259.9 nm, respectively.

2.2. Crystallization of SOD2

Crystals of both native SOD2 and Fe-substituted SOD2 were obtained at 288 K by the hanging-drop vapour-diffusion method. For crystallization, the protein concentration was 20 mg ml^{-1} in a buffer consisting of 20 m*M* Tris–HCl pH 7.5 and 200 m*M* NaCl. For the native Mn-SOD2, 1 µl protein solution was mixed with 1 µl reservoir solution consisting of 48% MPD, 0.1 *M* Tris–HCl pH 8.5 and 0.2 *M* $NH_4H_2PO_4$. For the Fe-substituted SOD2, the reservoir solution was 45% MPD, 0.1 *M* Bicine pH 9.5 and 0.2 *M* $NH_4H_2PO_4$. Cubic crystals with a maximal size of 0.2 mm on each side appeared within 2 d. For data collection, the crystals were frozen in liquid nitrogen after soaking in a cryoprotectant buffer consisting of 50% MPD, 0.1 *M* Tris–HCl pH 8.5 (0.1 *M* Bicine pH 9.5 for Fe-substituted SOD2), 0.2 *M* $NH_4H_2PO_4$.

2.3. Data collection and structure determination

The crystal was flash-frozen in a stream of nitrogen gas at 100 K. Diffraction data were collected using a Rigaku MicroMax-007 HF X-ray generator equipped with a MAR345dtb image plate (MAR Research, Germany) using a wavelength of 1.5418 Å and 1° oscillations. X-ray crystallographic data were processed using *iMOSFLM* (Battye *et al.*, 2011). The structure was determined by molecular replacement with the program *MOLREP* (Vagin & Teplyakov, 2010) using the structure of *Aspergillus fumigatus* Mn-SOD (PDB entry 1kkc; Flückiger *et al.*, 2002) as the search model. Crystallographic refinement was performed using *REFMAC*5 (Murshudov *et al.*, 2011). After several rounds of manual rebuilding using the program *Coot*

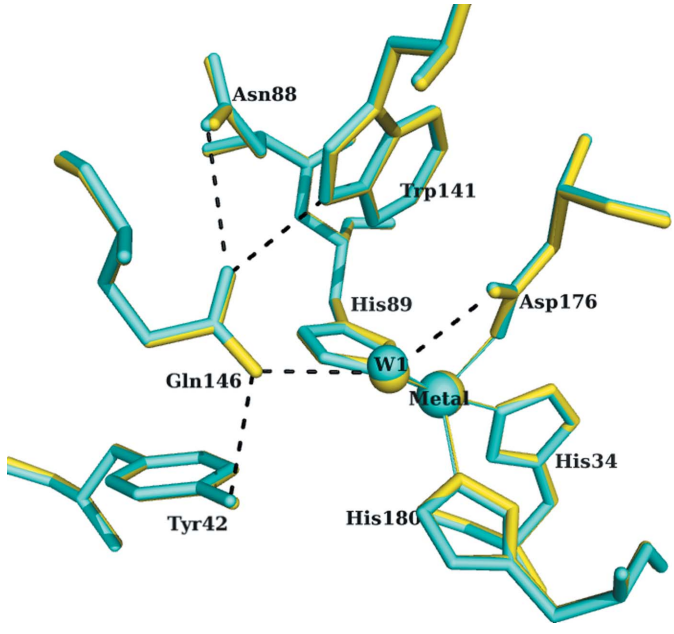

Figure 2
Superposition of the active site of the native SOD2 (cyan) onto that of the Fe-substituted SOD2 (yellow). The coordinated solvent is denoted W1. The hydrogen-bond network is denoted by black dashes.

(Emsley & Cowtan, 2004), the metal atom and water molecules were placed into the electron-density map, resulting in the final model. Structure factors and coordinates have been deposited in the Protein Data Bank (PDB entries 3bfr and 3rn4). The final statistics and refinement parameters are listed in Table 1. All structural figures were prepared using *PyMOL* (DeLano, 2002).

3. Results and discussion

3.1. The overall structure of SOD2 from *S. cerevisiae*

The crystal structures of both native SOD2 and Fe-substituted SOD2 have only one molecule per asymmetric unit. Two monomers related by a crystallographic twofold axis form a functional dimer. Briefly, each monomer consists of a long protruding α-helical domain (α1–α3) at the N-terminus; the remainder of the protein forms an α/β-domain with a central β-sheet (composed of β1–β3) surrounded by five α-helices (α4–α8) at the C-terminus (Fig. 1*a*). The metal ion lies between the two domains and is coordinated by the $N^{\varepsilon2}$ atoms of His34, His89 and His180, Asp176 $O^{\delta1}$ and a solvent molecule (Fig. 2). Although there is only one molecule in the asymmetric unit, the monomers assemble through the crystallographic symmetry axis to form tight tetramers from the 222 symmetry. The dimer interface is highly conserved in the Fe/Mn-SOD family and has been proposed to be involved in intersubunit cooperation (Muñoz *et al.*, 2005). Two dimers form a tetramer *via* interactions between the protruding α-helices and loops of the C-terminal domain. This tetramer interface is also very similar to those of the human (Guan *et al.*, 1998) and *A. fumigatus* (Flückiger *et al.*, 2002) enzymes.

As this was the first structure of SOD2 from *S. cerevisiae*, a *DALI* server (Holm & Rosenström, 2010) search was performed and revealed that Mn-SOD from *A. fumigatus* (PDB entry 1kkc; Flückiger *et al.*, 2002) was the most similar structure from other species, with the highest *Z* score of 29.9–30.0 and an r.m.s. deviation of 0.9 Å for 194 C^{α}-atom pairs. At the same time, another structure of SOD2 from *S. cerevisiae* was solved corresponding to the same protein but with Mn^{II} instead of Mn^{III} as in our structure. The overall r.m.s.d. between the two structures was 0.178–0.234 Å for 176–187 C^{α}-atom pairs.

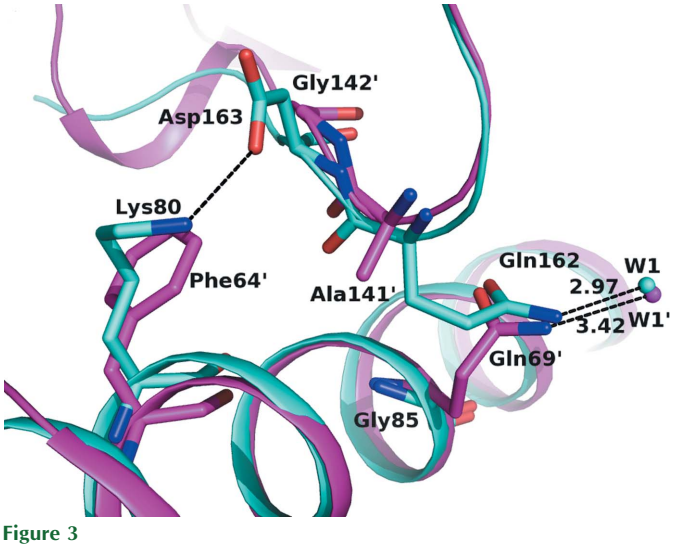

Figure 3
The hydrogen-bonding pair that is potentially responsible for the metal specificity of SOD2 (cyan). The Fe-specific SOD from *E. coli* (pink; PDB entry 1isa; Lah *et al.*, 1995) was superimposed onto SOD2 for comparison. Hydrogen bonds are denoted by black dashed lines; the hydrogen-bond distance between $N^{\varepsilon2}$ of Gln162/Gln69′ is also labelled to demonstrate the E_m tuning difference.

Table 2
Summary of the hydrogen-bond distances Gln162 $N^{\varepsilon2}\cdots$W1 in Mn-specific SODs and Gln69 $N^{\varepsilon2}\cdots$W1 in Fe-specific SODs available in the PDB.

(*a*) Mn-SODs.

PDB entry	3bfr†	1kkc	1noj	3mds	1xuq	1y67	1vew	1gv3	3lsu	Average
Gln162 $N^{\varepsilon2}\cdots$W1 distance (Å)	2.97	2.62	2.94	3.01	2.87	2.76	3.01	2.85	2.95	2.88

(*b*) Fe-SODs.

PDB entry	2gpc	2bpi	2cw2	1isa	1my6	2cw3	1unf	Average
Gln69 $N^{\varepsilon2}\cdots$W1 distance (Å)	3.36	3.39	3.18	3.42	3.28	3.53	3.18	3.33

† This study.

3.2. Comparison of Fe-substituted SOD2 with native SOD2

Fe-substituted SOD2 was prepared by culturing the transformant cells in minimum medium M9 supplemented with 0.1 m*M* $FeCl_3$. The purified protein was yellowish (indicating the presence of Fe^{3+} ions) and the molar ratio of manganese:iron was determined to be 5:95. The residual manganese ion in the protein most likely arose from impurities in the medium. Superposition of the structures of the Fe-substituted SOD2 and native SOD2 showed that (i) global structural alignment yields a root-mean-square deviation of only 0.08 Å for 189 C^{α} atoms and (ii) the hydrogen-bonding network around the metal atom also aligns very well (Fig. 2). The structural comparison of the two structures shows no significant conformational alteration in the overall structure or the active site upon binding the non-native metal iron.

3.3. Possible structural basis of the metal specificity of SOD2

The metal specificity of Fe/Mn-SOD has long been exploited and sequence alignment has revealed that the most prominent difference within 10 Å of the active site is that the role of Gln162 in Mn-specific SODs is performed by Gln69 in Fe-specific SODs (Hiraoka *et al.*, 2000). On one hand, both these residues form hydrogen bonds to the coordinated solvent and density-functional calculations have suggested that a higher degree of protonation of the coordinated solvent W1 can depress the mid-point potential (E_m) of the metal centre much more (Fisher *et al.*, 1996), thus finely tuning the E_m of the metal centre. Therefore, we summarized the Gln162 $N^{\varepsilon2}\cdots$W1 hydrogen-bond distances in the structures of Mn-specific SODs and the Gln69 $N^{\varepsilon2}\cdots$W1 hydrogen-bond distances in the structures of Fe-specific SODs available in the PDB (Table 2) and found that the distance is significantly longer (0.4 Å on average) in Fe-specific SODs than in Mn-specific SODs, suggesting that the degree of protonation of solvent W1 is higher in Mn-specific SODs than in Fe-specific SODs, resulting in the E_m of the manganese ion being depressed much more than that of the iron ion. It can also be deduced that the E_m of the metal centre can either be raised or lowered by altering the distance between the $N^{\varepsilon2}$ atom of Gln162/Gln69 and the coordinated solvent; thus, the metal specificity can be monitored. On the other hand, the sequence fingerprint in the vicinity of Gln162 and Gln69 is distinct between Mn-specific and Fe-specific SODs (Fig. 1*b*): Gln69 of Fe-specific SODs lies in a characteristic A(A/G)Q(I/V)(F/W/Y) peptide of helix α3, while the equivalent region of Mn-specific SODs is (G/A)GG(H/F)*X* (where *X* denotes any amino acid). Gln162 of

Mn-specific SOD lies in a loop region which has a variable length among different species. Two residues, Asp163 and Lys80, are only well conserved in Mn-specific SODs and form hydrogen bonds through their side chains to stabilize the loop region so that Gln162 $N^{\varepsilon 2}$ can be placed in a favourable orientation for solvent (W1) governing (Fig. 3). Hence, Asp163 and Lys80 may be potential targets for engineering/altering the metal specificity of Mn-SODs.

3.4. Electrostatic potential distribution of SOD2 and structural implications for its high catalytic efficiency

The electrostatic potential surface of the SOD2 dimer was calculated to qualitatively demonstrate the surface-charge properties of the protein (Fig. 4*a*). Interestingly, most parts of the protein surface are negatively charged, except for a zone in the proximity of a funnel-shaped substrate-access channel at the dimer interface (Parker & Blake, 1988). This is quite similar to the case in Cu/Zn-SODs; that is, although dimeric Cu/Zn-SODs have a negative net charge overall, a positive electrostatic potential field surrounds the active centre to guide the superoxide anion to access the active site (Bordo *et al.*, 1999). Wholly unlike the Cu/Zn-SODs, the substrate-access channel of SOD2 is narrower and deeper and the bottom of the funnel is peculiarly negatively charged. Further inspection of the structure of SOD2 reveals that the dimer's funnel is formed by part of helix α2 near the N-terminus of one subunit and the loops between helix α5 and strand β1 and between helix α6 and helix α7 of the other subunit. The major contribution to the positively charged surface around the funnel comes from Lys37 and His38 of one subunit and Asn188 and Lys190 of the other subunit (Fig. 4*b*). These four residues are the same as in human Mn-SOD (Borgstahl *et al.*, 1992), with the exception that Lys190 is substituted by Arg190. It is worth noting that these four residues are highly conserved in the Mn/Fe-SOD family. Thus, as in the Cu/Zn-SODs, the positive electrostatic zone of Mn/Fe-SOD around the active site is essential for the extremely high catalytic efficiency of the enzyme by attracting the negatively charged substrate anion $O_2^{-\cdot}$ towards the metal centre to facilitate the enzyme–substrate encounter.

In conclusion, we have determined the crystal structures of both native SOD2 and Fe-substituted SOD2 from *S. cerevisiae*, which share the same fold and align very well. Statistical comparisons revealed that the Gln69···W1 hydrogen-bond length in Fe-specific SODs is 0.4 Å longer than the Gln162···W1 hydrogen-bond length in Mn-specific SODs, suggesting that Gln162/Gln69 may play an essential role in metal specificity. The residues Asp163 and Lys80 have been proposed to potentially be responsible for the metal specificity of Mn-specific SODs. The electrostatic potential surface of SOD2 revealed a conserved positively charged electrostatic zone that possibly functions by pushing the negatively charged $O_2^{-\cdot}$ anion towards the active-site metal.

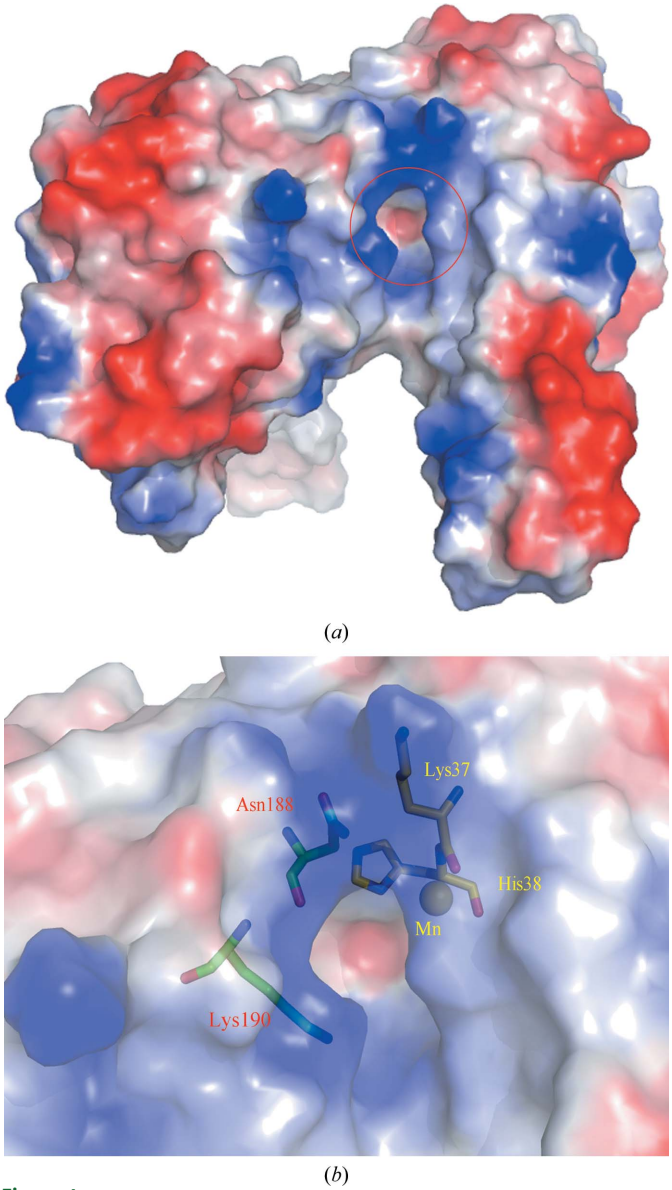

(*a*)

(*b*)

Figure 4
Positive electrostatic potential zone around the substrate-access funnel. (*a*) The electrostatic surface of the SOD2 dimer. The regions of the surface that have positive electrostatic potential are coloured blue and those that have negative potential are coloured red. The substrate-access funnel is highlighted by a red circle. (*b*) A close-up view of the substrate-access funnel. The residues that account for the attractive electrostatic zone are shown as sticks and the different colours of the residue labels indicate that they are from different subunits. The electrostatic potential of the protein surface was calculated using *PyMOL*.

We are grateful to the developers of the *CCP*4 suite, *ESPript*, *MolProbity* and *PyMOL*. This work was supported by projects 2006CB910202 and 2006CB806501 of the Ministry of Science and Technology of China and grant 30870490 from the Chinese National Natural Science Foundation.

References

Battye, T. G. G., Kontogiannis, L., Johnson, O., Powell, H. R. & Leslie, A. G. W. (2011). *Acta Cryst.* D**67**, 271–281.
Beyer, W. F. & Fridovich, I. (1991). *J. Biol. Chem.* **266**, 303–308.
Bordo, D., Matak, D., Djinovic Carugo, K., Rosano, C., Pesce, A., Bolognesi, M., Stroppolo, M. E., Falconi, M., Battistoni, A. & Desideri, A. (1999). *J. Mol. Biol.* **285**, 283–296.
Borgstahl, G. E., Parge, H. E., Hickey, M. J., Beyer, W. F., Hallewell, R. A. & Tainer, J. A. (1992). *Cell*, **71**, 107–118.
DeLano, W. L. (2002). *PyMOL*. http://www.pymol.org.
Emsley, P. & Cowtan, K. (2004). *Acta Cryst.* D**60**, 2126–2132.
Fisher, C. L., Chen, J.-L., Li, J., Bashford, D. & Noodleman, L. (1996). *J. Phys. Chem.* **100**, 13498–13505.
Flückiger, S., Mittl, P. R., Scapozza, L., Fijten, H., Folkers, G., Grütter, M. G., Blaser, K. & Crameri, R. (2002). *J. Immunol.* **168**, 1267–1272.
Guan, Y., Hickey, M. J., Borgstahl, G. E., Hallewell, R. A., Lepock, J. R., O'Connor, D., Hsieh, Y., Nick, H. S., Silverman, D. N. & Tainer, J. A. (1998). *Biochemistry*, **37**, 4722–4730.
Hiraoka, B. Y., Yamakura, F., Sugio, S. & Nakayama, K. (2000). *Biochem. J.* **345**, 345–350.

Holm, L. & Rosenström, P. (2010). *Nucleic Acids Res.* **38**, W545–W549.
Lah, M. S., Dixon, M. M., Pattridge, K. A., Stallings, W. C., Fee, J. A. & Ludwig, M. L. (1995). *Biochemistry*, **34**, 1646–1660.
Luk, E., Carroll, M., Baker, M. & Culotta, V. C. (2003). *Proc. Natl Acad. Sci. USA*, **100**, 10353–10357.
Muñoz, I. G., Moran, J. F., Becana, M. & Montoya, G. (2005). *Protein Sci.* **14**, 387–394.
Murshudov, G. N., Skubák, P., Lebedev, A. A., Pannu, N. S., Steiner, R. A., Nicholls, R. A., Winn, M. D., Long, F. & Vagin, A. A. (2011). *Acta Cryst.* D**67**, 355–367.
Parker, M. W. & Blake, C. C. (1988). *J. Mol. Biol.* **199**, 649–661.
Vagin, A. & Teplyakov, A. (2010). *Acta Cryst.* D**66**, 22–25.
Yang, M., Cobine, P. A., Molik, S., Naranuntarat, A., Lill, R., Winge, D. R. & Culotta, V. C. (2006). *EMBO J.* **25**, 1775–1783.